Science Letters ISSN 2345-5463 DOI: https://doi.org/10.47262/SL/10.3.132022200

Research article
2022 | Volume 10 | Issue 3 | Pages 95-105

ARTICLE INFO

Received
May 16, 2022
Revised
July 29, 2022
Accepted
August 02, 2022
Published
September 14, 2022

***Corresponding author**
Oluwatoba E. Oyeneyin
Email
oluwatoba.oyeneyin@aaua.edu.ng
emmanueltoba90@gmail.com

Keywords
Triazolopyrimidinones
Corrosion inhibitors
Density functional theory
Electronic properties
Reactivity descriptors
Monte Carlo simulation

How to cite
Oyeneyin OE. Investigation of corrosion inhibition potential of triazolopyrimidinone via density functional theory and Monte-Carlo stimulation. Sci Lett 2022; 10(3):95-105

Open Access

Investigation of Corrosion Inhibition Potential of Triazolopyrimidinones via Density Functional Theory and Monte-Carlo Simulations

Oluwatoba Emmanuel Oyeneyin*

Theoretical and Computational Chemistry Unit, Department of Chemical Sciences, Adekunle Ajasin University, Akungba-Akoko, Ondo State, Nigeria

Abstract

The protection of metal parts from corrosion is important to save the cost of production of goods and lives. Twelve triazolopyrimidinone derivatives were investigated for their ability to inhibit the corrosion of metal via density functional theory and Monte Carlo (MC) simulation approaches. The electronic properties and global and local reactivity descriptors were computed at the B3LYP/6-31G(d) level of theory, using Spartan 14 software. The Mulliken charge distribution and electrostatic potential (ESP) maps were used to locate the reactive sites. The adsorption of the compounds on the surface of the stable Fe(110) was investigated in an aqueous solution using the adsorption locator module on Material Studio software. The values of energies of their frontier molecular orbitals and other reactivity descriptors suggest that these molecules displayed good corrosion inhibition potentials. The Mulliken charge distribution and electrostatic potential maps showed that they can donate electrons to the metal and at the same time accept electrons via back-donation, also rationalized by the values of their electron back-donation calculated. The molecules interacted well with Fe(110) surface in an aqueous medium, as revealed by the MC results.

SCAN ME

Introduction

The use of metals in construction materials, oil and gas, and petroleum industries is very common. They, however, readily undergo degradation via chemical or electrochemical reactions with their surroundings [1], this is because they are thermodynamically unstable in their pure forms. Corrosion is a major issue that has affected several industries worldwide, destabilizing the world economy. It has resulted in the breakage of oil and underground water pipes, failure of bridges, contamination of products from leakages of pipes, damage of metallic equipment, and contamination of air through the release of harmful pollutants from iron corrosion [2]. In 2013, the cost of corrosion globally was estimated to be 2.5 trillion US dollars, which is around 3-4% of the global GDP [3]. Some of the metal materials come in contact with acids used during prickling, descaling, and oil well acidizing [4, 5]. Corrosion is a natural process that cannot be eliminated but can be mitigated by adopting some approaches. These approaches include modification of metal/alloy, prevention of surface reactions (anodic and cathodic methods, protective coatings, modification of surface conditions, and the inhibition of surface corrosion (use of corrosion inhibitors) [6, 7]. The use of corrosion inhibitors is the most cost-effective and efficient way of mitigating corrosion.

Corrosion inhibitor has been extensively used in mitigating corrosion in many industrial sectors. It is a liquid or solid substance which reduces the rate of corrosion when added to a suitable concentration without significantly changing the concentration of the corrosive agent [8, 9]. Corrosion inhibitors could be organic or inorganic inhibitors. The use of organic corrosion inhibitors is most preferred due to their high efficiency, less toxicity, and being eco-friendly and cheaply available [10, 11]. The efficacy of organic corrosion inhibitors usually depends on the presence of heteroatoms including oxygen, nitrogen, and phosphorous, and pi-electron which enables them to be adsorbed on the metal surface forming a barrier between the metal surface and environment and protecting the surface from an acidic environment [10, 12]. The adsorption of inhibitors on a metal surface can either be chemisorption (involving the interaction between the lone pairs of the molecule and the vacant *d*-orbital of the metal to form a coordinate bond) or physisorption (involving the electrostatic interaction between the molecule and the electrically charged metal surface) [13].

Triazolopyrimidinone is a heterocyclic molecule that comprises triazole and fused pyrimidinone/4-hydoxylpyrimidine rings [14, 15]. Triazolopyrimidine compounds have been widely used in medicinal chemistry for their various therapeutic properties [16]. Triazolopyrimidine derivatives have been reported to possess antibacterial, antitumor, and anti-malaria activities. Due to the presence of heteroatoms (N, S that can donate an electron to the metal surface, fully conjugated pi-electron, its derivatives could act as potential anti-corrosive candidates. The corrosion inhibition efficiency of a compound can be effectively measured via experimental means. However, because of cost and time, theoretical methods are now employed to first investigate these molecules before laboratory experiments.

Density functional theory (DFT) is a powerful tool employed to investigate the electronic properties of a molecule [17]. DFT provides insight into the transfer and distribution of electrons when molecules interact with a metal's surface. It has proven a very effective and accurate method of predicting the properties of molecules [18, 19], including corrosion inhibition potentials [20, 21]. Furthermore, the Monte Carlo (MC) simulation explains a molecule's orientation and mechanism of adsorption on the metal surface [22]. It predicts the adsorption energy when an inhibitor adsorbs on the surface of a metal. Therefore, this work investigated the corrosion inhibitive potentials of some triazolopyrimidinone derivatives (Fig. 1) using DFT and Monte Carlo simulation. These molecules were earlier reported by Istanbullu and coworkers as antimicrobial agents [16].

Methods

Quantum chemical calculations

Optimization of the structures of triazolopyrimidinone derivatives (A1-A6, B1-B6) was performed at the DFT/B3LYP/6-31G* level of theory on Spartan 14 software [23] having initially obtained the global minima (most stable conformers) [24]. All DFT calculations were done in the gas phase. The quantum parameters were calculated (equations 1-9) as described earlier [25].

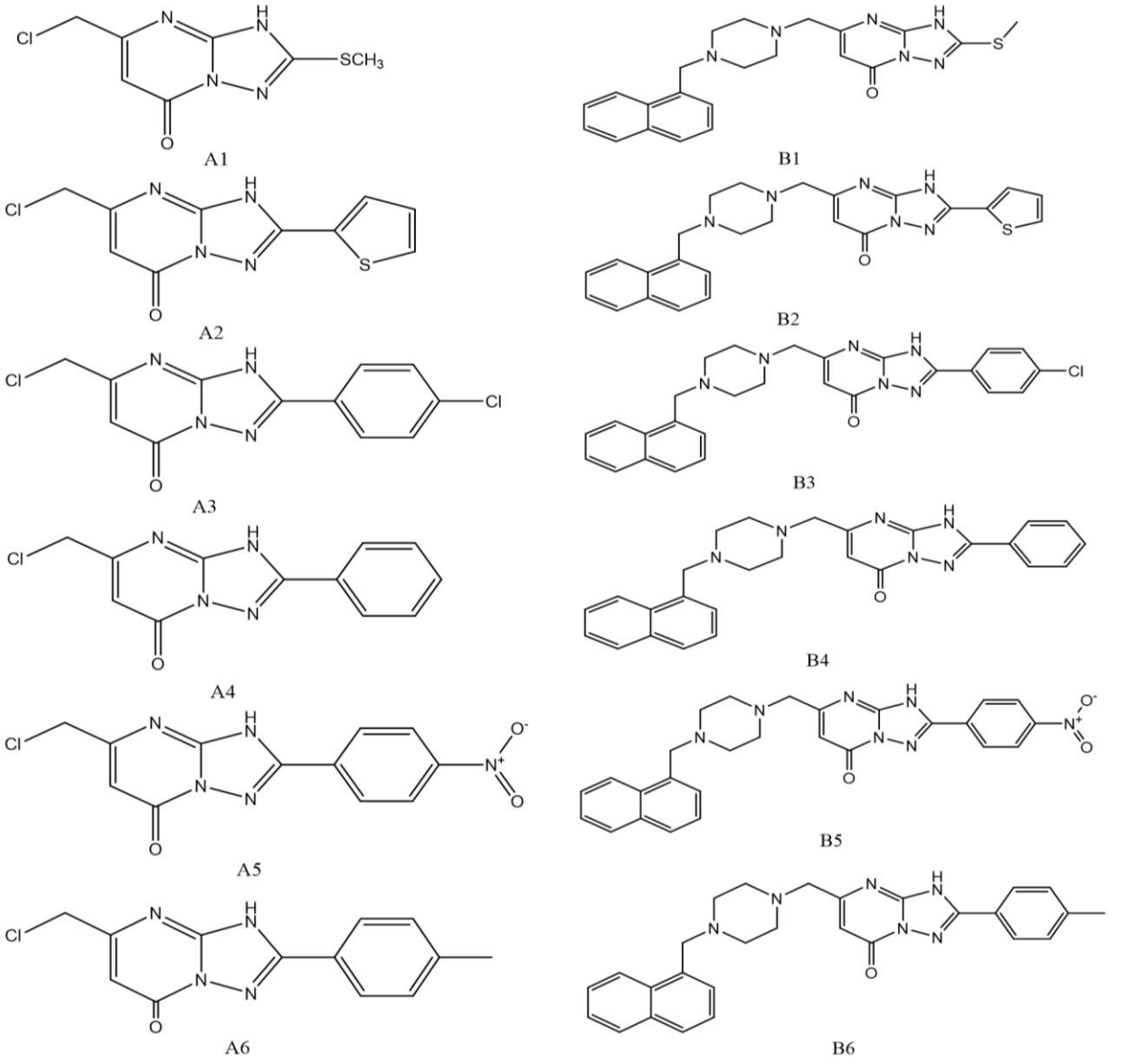

Fig. 1 Structures of the Triazolopyrimidinone derivatives under investigation.

A1 = 3*H*-5-(Chloromethyl)-2-(metylthio)-[1,2,4]triazolo[1,5-*a*]pyrimidine-7-one
A2 = 3*H*-5-(Chloromethyl)-2-(thiophene-2-yl)-[1,2,4]triazolo[1,5-*a*]pyrimidine-7-one
A3 = 3*H*-5-(Chloromethyl)-2-(4-chlorophenyl)-[1,2,4]triazolo[1,5-*a*]pyrimidine-7-one
A4 = 3*H*-5-(Chloromethyl)-2-phenyl-[1,2,4]triazolo[1,5-*a*]pyrimidine-7-one
A5 = 3*H*-5-(Chloromethyl)-2-(4-nitrophenyl)-[1,2,4]triazolo[1,5-*a*]pyrimidine-7-one
A6 = 3*H*-5-(Chloromethyl)-2-(4-methylphenyl)-[1,2,4]triazolo[1,5-*a*]pyrimidine-7-one
B1 = 3*H*-2-(Methylthio)-5-((4-(naphthalen-1-ylmethyl)piperazin-1-yl)methyl)-[1,2,4]triazolo[1,5 *a*]pyrimidin-7-one
B2 = 3*H*-5-((4-(Naphthalen-1-ylmethyl)piperazin-1-yl)methyl)-2-(thiophen-2-yl)-[1,2,4]triazolo[1,5 *a*]pyrimidin-7-one
B3 = 3*H*-2-(4-Chlorophenyl)-5-((4-(naphthalen-1-ylmethyl)piperazin-1-yl)methyl)-[1,2,4]triazolo[1,5- *a*]pyrimidin-7-one
B4 = 3*H*-5-((4-(Naphthalen-1-ylmethyl)piperazin-1-yl)methyl)-2-phenyl-[1,2,4]triazolo[1,5-*a*]pyrimidin-7-one
B5 = 3*H*-5-((4-(Naphthalen-1-ylmethyl)piperazin-1-yl)methyl)-2-(4-nitrophenyl)-[1,2,4]triazolo[1,5-*a*]pyrimidin-7-one
B6 = 3*H*-5-((4-(Naphthalen-1-ylmethyl)piperazin-1-yl)methyl)-2-(*p*-tolyl)-[1,2,4]triazolo[1,5-*a*]pyrimidin-7-one

$$E_g = E_{LUMO} - E_{HOMO} \quad \text{eq. 1}$$

$$I = -E_{HOMO} \quad \text{eq. 2}$$

$$A = -E_{LUMO} \quad \text{eq. 3}$$

$$\chi = \frac{I+A}{2} \quad \text{eq. 4}$$

$$\eta = \frac{I-A}{2} \quad \text{eq. 5}$$

$$\delta = \frac{1}{\eta} \quad \text{eq. 6}$$

$$\omega = \frac{\chi^2}{2\eta} \quad \text{eq. 7}$$

$$\Delta N = \frac{X_{metal}-X_{inh}}{2(\eta_{Fe}+\eta_{inh})} \quad \text{eq. 8}$$

$$\Delta E_{back-donation} = -\frac{\eta}{4} \quad \text{eq. 9}$$

The local reactivity descriptors of the molecules can be obtained using the Fukui function calculation. The Fukui function provides insight into the region where nucleophilic and electrophilic attacks occur in a molecule [26]. Charge of an atom in the neutral q(N), anionic q(N+1), and cationic q(N−1) states, that the Fukui functions can be uniquely calculated using equations 10-12.

$$f_k^+ = [qk(N + 1)- qk(N)] \text{ (nucleophilic attack)} \quad \text{eq. 10}$$

$$f_k^- = [qk(N) - qk(N-1)] \text{ (electrophilic attack)} \quad \text{eq. 11}$$

$$\Delta f_k(r) = f_k^+ - f_k^- \quad \text{eq. 12}$$

Monte Carlo simulation

Compounds A1-6 and B1-6 were simulated using the Monte Carlo method to assess the adsorption and possible interactions between them and Fe(110) surface along the low-index miller facet [8, 22, 25]. Fe (110) plane was selected for its good stability and well-packed structure [27]. The molecules and Fe (110) were optimized using the Forcite module as earlier described [8, 25]. In a bid to mimic the experiment, the simulation was done in an aqueous environment by including water molecules. Adsorption of the molecules was done using the COMPASS force field in the adsorption locator module to obtain the adsorption energy (E_{Ads}) and the deformation energy (E_{Def}) in kcal/mol [22].

Results and Discussion

Corrosion inhibition, frontier orbital energies, and reactivity descriptors

The assessment of reactivity of the molecules is established on the frontier molecular orbitals energy (FMOs) theory of Fukui. The FMOs energies, that is, E_{HOMO} (energy of highest occupied molecular orbital) and E_{LUMO} (energy of unoccupied molecular orbital) are important quantum properties used to describe the reactivity of a molecular system. E_{HOMO} and E_{LUMO} help in pointing out the orbitals that can donate and those that can accept electrons in a molecule. These energies help in predicting the corrosion inhibitory performance of molecules. E_{HOMO} explains the ability of molecules to donate electrons. The HOMO energies ranged from (-6.42 to -5.63 eV) of the molecules follow the following trend: B6 > B4 = B2 > B1 > B5 > B3 > A6 > A2 > A4 > A1 > A3 > A5 (Table 1). Molecule B6 has the highest HOMO energy (-5.63 eV) and the highest ability to donate electrons, that is the energy required by it to donate an electron is the lowest (ionization potential of 5.63 eV), while A5 has the lowest HOMO energy (-6.42 eV) and, hence, the highest number of ionization potential, making it the least ready to give up an electron [28]. The electron accepting ability of a molecule is described by the E_{LUMO} value, low E_{LUMO} value favors a high potential of electron acceptance [7]. The E_{LUMO} of the molecules follow the following trend: B1 > A1 > B2 > B6 > B4 > A2 > A6 > A4 > B3 > A3 > B5 > A5. Molecule B1 has the highest LUMO (-0.94 eV), hence the lowest ability to accept an electron that is its electron affinity is the lowest (0.94 eV), while A5 has the lowest LUMO (-3.04 eV), hence the highest electron affinity (3.04 eV) [28]. The Energy band gap (E_g) explains the reactivity and stability of a molecule during adsorption on a metal surface. A lower value in E_g indicates an increase in the reactivity of a molecule, enabling improved inhibitory effects while the higher value of E_g indicates high chemical stability, leading to a decrease in inhibitory effect [29]. The E_g values for the studied compound are of the order: A1 > B1 > A2 > A6 > A4 > A3 > B2 > B6 > B4 > B3 > A5 > B5 (Table 1). Generally, the molecular orbitals of molecules B1-B6 are more stabilized over their A series due to the higher molecular size of each counterpart. This also led to a decrease in

Table 1 Electronic parameters and reactivity descriptors of the compounds: frontier molecular orbital energies (E_{HOMO} and E_{LUMO}), ionization potential (I), electron affinity (A), electronegativity (χ), chemical hardness (ηV), chemical softness (δ), electrophilicity (ω), fraction of electron transferred (ΔN) and electron back-donation ($\Delta E_{back-donation}$). All values were calculated at the B3LYP/6-31G(d) level of theory.

Compounds	E_{HOMO} (eV)	E_{LUMO} (eV)	E_g (eV)	I (eV)	A (eV)	χ (eV)	η (eV)	δ (eV^{-1})	ω (eV)	ΔN	$\Delta E_{back-donation}$
A1	-6.20	-1.30	4.90	6.20	1.30	3.75	2.45	0.41	2.87	0.66	-0.61
A2	-6.12	-1.70	4.42	6.12	1.70	3.91	2.21	0.45	3.45	0.69	-0.55
A3	-6.25	-2.04	4.21	6.25	2.04	4.15	2.11	0.48	4.08	0.68	-0.53
A4	-6.13	-1.82	4.31	6.13	1.82	3.97	2.15	0.46	3.66	0.70	-0.53
A5	-6.42	-3.04	3.38	6.42	3.04	4.73	1.69	0.59	6.61	0.67	-0.42
A6	-6.08	-1.72	4.36	6.08	1.72	3.90	2.18	0.45	3.48	0.71	-0.54
B1	-5.66	-0.94	4.72	5.66	0.94	3.30	2.36	0.42	2.30	0.78	-0.59
B2	-5.64	-1.49	4.15	5.64	1.49	3.56	2.07	0.48	3.06	0.82	-0.51
B3	-5.68	-1.86	3.82	5.68	1.86	3.77	1.91	0.52	3.70	0.84	-0.47
B4	-5.64	-1.60	4.04	5.64	1.60	3.62	2.02	0.49	3.24	0.83	-0.50
B5	-5.71	-2.94	2.77	5.71	2.94	4.32	1.38	0.72	6.74	0.96	-0.34
B6	-5.63	-1.51	4.12	5.63	1.51	3.57	2.06	0.49	3.09	0.83	-0.52

the energy band gaps of molecules B1-B6 over their corresponding A analogs. For example, A5 has 3.38 eV while its analog B5 has 2.77 eV. From both series, the nitro group resulted in the lowering of the energy band gap, as was observed in the literature [30], but was lower in A5 as a result of higher molecular size. Compound B5 has the lowest band gap energy indicating that it is the most reactive, therefore could possess better corrosion inhibition potentials than other compounds under investigation. The low energy band gap values of A5 and B5 are due to the attachment of electron-withdrawing nitro groups in the structures; nitro-substituted molecules are usually characterized by low energy band gaps [30].

Global reactivity descriptors are important parameters used in describing and predicting the inhibitory effect of potential inhibitors. The electronic properties and global reactivity descriptors of the molecules are presented in Table 1. A maximum ionization potential signifies that the compound has a low electron donating ability, while a low ionization potential signifies a high electron acceptance ability [12, 31]. Compounds B6, B4, and B2 displayed the lowest ionization energy (5.63, 5.64 and 5.64 eV, respectively) indicating the high electron-releasing potential of the compounds. Electronegativity (χ) is the ability of an atom in a molecule to attract electrons toward itself [32]. Lower electronegativity values enable molecules to easily accomplish electron equilibrium, increasing their reactivity. The electronegativity values of the studied compounds, as shown in Table 1, are in the range of 3.30 eV – 4.32 eV with compound G showing the lowest electronegativity value. The global hardness (η) and softness (δ) are determined in compliance with the HSAB theory [33]. The theory says that the compounds prefer to bind with systems where they pose the same or similar hardness (softness) and the rise in interaction energy occurs with a decrease in hardness and increase in softness [34]. Since hardness is directly from the energy band gap, B3, A5, and B5 have the lowest chemical hardness and chemical softness. (1.91 eV, 1.69 eV and 1.38 eV) and softness value (0.52 eV^{-1}, 0.59 eV^{-1} and 0.72 eV^{-1}).

Energy stabilization via the flow of electrons is measured by the value of global electrophilicity. Nucleophiles possess low electrophilicity. Molecule B1 is the best nucleophile while B5 is the best electrophile. Furthermore, molecules are absorbed into the metal surface by donating /transferring electrons. Transferring more electrons enhances inhibition efficiency. The electron transfer (ΔN) number indicates better interaction between the molecule and metal surface since they are all less than 3.6 [25]. The ΔN values shown in Table 1 follow the order: B5 > B3 > B4 = B6 > B2 > B1 > A6 > A4 > A2 > A3 > A5 > A1. Negative values of $\Delta E_{back-donation}$ displayed by all molecules indicate that charge transfer between the surface of the metals and the molecules is energetically favored, implying that all molecules can make electrons available via

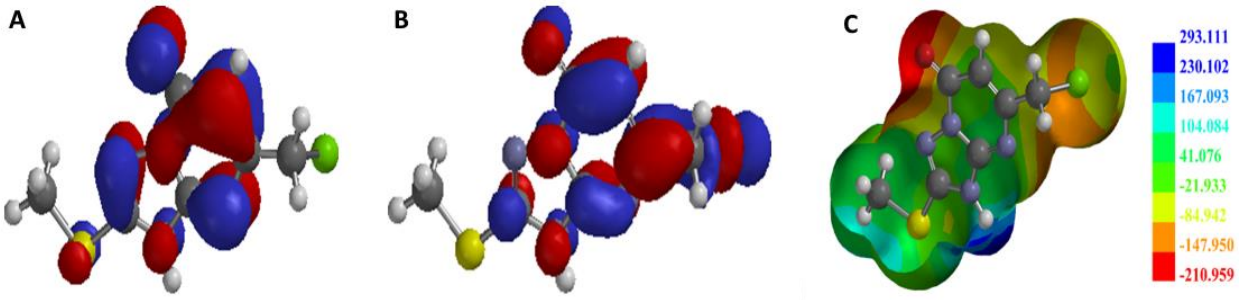

Fig. 2 HOMO map (**A**), LUMO map (**B**) and electrostatic potential map (**C**) of triazolopyrimidinone derivative A1.

back-donation [35].

Surfaces (HOMO, LUMO and electrostatic potential maps)

The HOMO, LUMO and electrostatic potential (ESP) maps of compound A1 are displayed in Fig. 2. Figs. S1-S11 show the HOMO, LUMO and electrostatic potential (ESP) maps of compounds A2, A3, A4, A5, A6, B1, B2, B3, B4, B5 and B6. The HOMO of A1 spreads across the entire molecule, leaving out the chloromethyl and the methyl on the thiomethyl groups (Fig. 2a), while the LUMO covers the same regions, adding the chloromethyl group and leaving out the entire thiomethyl group (Fig. 2b). The ESP map of A1 indicates that the carbonyl oxygen (red) on the pyrimide-7-one and chloromethyl (yellow and orange) regions are the sites that will mostly favor electrophilic attack while the triazole hydrogen, sulfur on methylthiol group, triazole and pyrimidine ring favor nucleophilic attack (Fig. 2c). The carbonyl oxygen and the triazole hydrogen are the best sites for electrophilic and nucleophilic attacks, respectively. The HOMO map of compounds A2 covers the triazole and pyrimidine rings (Fig. S1a), while the LUMO covers the thiophene-2-yl and parts of the triazole and pyrimidine rings, leaving out the chloromethyl group (Fig. S1b). The ESP map of A2 indicates that the carbonyl oxygen (red) on the pyrimide-7-one and chloromethyl (yellow and orange) regions are the sites that will mostly favor electrophilic attack while the triazole hydrogen, entire thiophene group, triazole and pyrimidine ring favor nucleophilic attack (Fig. S1c). The HOMO map of compound A3 covers the entire molecule except for the chlorophenyl and chloromethyl groups (Fig. S2a) while the LUMO covers majorly the chlorophenyl and triazole rings (Fig. S2b). The ESP map of A3 indicates that the carbonyl oxygen (red) on the pyrimide-7-one is the site that will mostly favor electrophilic attack while other regions will favor nucleophilic attack (Fig. S2c). The HOMO map of compounds A4 covers the triazole and pyrimidine rings (Fig. S3a), while the LUMO covers the phenyl, triazole and part of the pyrimidine ring (Fig. S3b). The ESP map of A4 indicates that the carbonyl oxygen (red) on the pyrimide-7-one and the chloromethyl (orange and yellow) are the sites that will mostly favor electrophilic attack while other regions will favor nucleophilic attack, with the most preferred being the triazole hydrogen (Fig. S3c). The HOMO map of compound A5 covers the triazole and pyrimidine rings (Fig. S4a), while the LUMO covers the nitrophenyl ring (Fig. S4b). The ESP map of A5 indicates that the carbonyl oxygen (red) on the pyrimide-7-one, nitro group on the nitrophenyl ring (yellow) and the chloromethyl (orange and yellow) are the sites that will mostly favor electrophilic attack while other regions will favor nucleophilic attack, with the most preferred being the triazole hydrogen (Fig. S4c). The HOMO map of compound A6 covers the triazole and pyrimidine rings (Fig. S5a), while the LUMO covers the entire molecule (Fig. S5b). The ESP map of A6 indicates that the carbonyl oxygen (red) on the pyrimide-7-one and the chloromethyl (orange and yellow) are the sites that will mostly favor electrophilic attack while other regions will favor nucleophilic attack, with the most preferred being the triazole hydrogen (Fig. S5c).

For B1-B6, the HOMO and LUMO of B1 spread across the naphthalene-1-ylmethyl group (Figs. S6a and b). The ESP map of B1 indicates that the triazole and pyrimidine rings (red) are the sites mostly preferred for the electrophilic attack while the triazole hydrogen and other regions favor nucleophilic attack (Fig. S6c). The HOMO of B2 covers the naphthalene-1-ylmethyl group (Fig.

Table 2 Charges on the anionic, neutral and cationic species qk (N+1), qk (N) and qk (N-1), respectively. The Fukui charges for nucleophilic (fk^+) and electrophilic attack (fk^-) and the Fukui function (Δf_K) on triazolopyrimidinone derivative A1.

Atom	q_k (N+1)	q_k	q_k (N-1)	f_k^+	f_k^-	Δf_k
C1	0.366	0.326	0.315	0.04	0.011	0.029
C2	-0.305	-0.276	-0.193	-0.029	-0.083	0.054
C3	0.508	0.622	0.653	-0.114	-0.031	-0.083
O1	-0.562	-0.494	-0.345	-0.068	-0.149	0.081
N1	-0.451	-0.442	-0.405	-0.009	-0.037	0.028
C4	0.787	0.818	0.845	-0.031	-0.027	-0.004
N2	-0.598	-0.56	-0.469	-0.038	-0.091	0.053
C5	-0.332	-0.436	-0.446	0.104	0.01	0.094
Cl1	-0.729	-0.075	0.01	-0.654	-0.085	-0.569
N3	-0.289	-0.275	-0.202	-0.014	-0.073	0.059
C6	0.32	0.329	0.332	-0.009	-0.003	-0.006
N4	-0.714	-0.708	-0.672	-0.006	-0.036	0.03
S1	0.126	0.181	0.393	-0.055	-0.212	0.157
C7	-0.577	-0.588	-0.66	0.011	0.072	-0.061

S7a) while the LUMO covers the thiophene, triazole and part of the pyrimidine rings (Fig. S7b). The ESP map of B2 indicates that the major electrophilic sites are the carbonyl oxygen (red) on the pyrimide-7-one with other parts in yellow and orange also favors electrophilic attack while other parts favor nucleophilic attack (Fig. S7c). The HOMO of B3 covers the same region as in B2 (Fig. S8a), while the LUMO covers the chlorophenyl, triazole and some parts of the pyrimidine rings (Fig. S8b). The ESP map of B3 indicates that the carbonyl oxygen (red) on the pyrimide-7-one is the site that will mostly favor electrophilic attack while other regions will favor nucleophilic attack (Fig. S8c). The HOMO of B4 covers the same region as in B2 and B3 (Fig. S9a), while the LUMO covers the phenyl, triazole and part of the pyrimidine ring (Fig. S9b). The ESP map of B4 indicates that the carbonyl oxygen (red) on the pyrimide-7-one and part of the pyrimidine ring (yellow) are the sites that will mostly favor electrophilic attack while other regions (the phenyl, triazole and naphthalene-1-ylmethyl groups) favor nucleophilic attack, with the most preferred being the triazole hydrogen (Fig. S9c). The HOMO of B5 covers some part of the naphthalene-1-ylmethyl group (Fig. S10a), while the LUMO covers the nitrophenyl ring (Fig. S10b). The ESP map of B5 indicates that the carbonyl oxygen (red) on the pyrimide-7-one, some parts of the pyrimidine ring and the naphthalene-1-ylmethyl group (yellow, red and orange) favor electrophilic attack while other regions will favor nucleophilic attack (Fig. S10c). The HOMO of B6 covers the naphthalene-1-ylmethyl group (Fig. S11a), while the LUMO covers the methylbenzene, triazole and some parts of the pyrimidine rings (Fig. S11b). The ESP map of B6 indicates that the carbonyl oxygen (red) on the pyrimide-7-one and some parts of the naphthalene ring (yellow) are the sites that will mostly favor electrophilic attack while other regions will favor nucleophilic attack, with the most preferred being the triazole hydrogen (Fig. 11S5c). The molecules all have sites that can accept and donate electrons, implying that they can bind to the surface of the metal via donation and back-donation of electrons, a rationalization of their probable use as corrosion inhibitors.

Local reactivity descriptors and charge distribution

The reactive sites on the compounds could be determined by the Mulliken charge distribution. Equations 10-12 show the calculated charges at the cationic, neutral and anionic levels (Tables 2 and S1 –S11). Electrophilic atoms are characterized by positive Δf_k values, while nucleophilic atoms are characterized by negative Δf_k values. The favorite nucleophilic site for molecule A1 is atom C5 (Table 2) with the highest value of f_k^+ (0.104) and a positive Δf_k value (0.094), while the favorite electrophilic site is atom C7 with f_k^- (0.072) and a negative Δf_k value (-0.061). The favorite nucleophilic site for molecule A2 is atom C5 (Table S1) with the highest value of f_k^+ (0.104) and

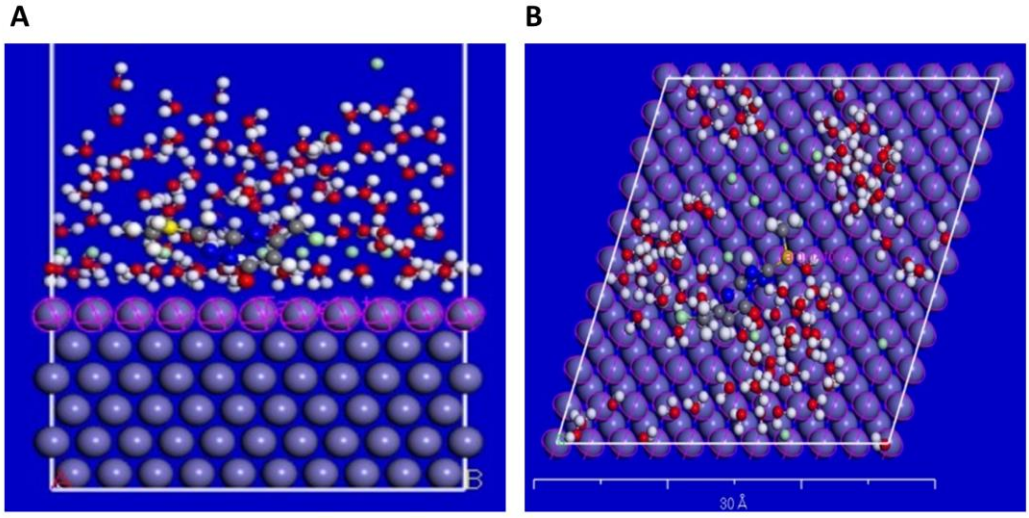

Fig. 3 Side view (**A**) and top view (**B**) of adsorption of triazolopyrimidinone derivative A1on Fe(110).

a positive Δf_k value (0.096) while the favorite electrophilic site is atom C7 with f_k^- (0.023) and a negative Δf_k value (-0.013). The favorite nucleophilic site for molecule A3 is atom C5 (Table S2) with the highest value of f_k^+ (0.103) and a positive Δf_k value (0.096), while the favorite electrophilic site is atom C7 with f_k^- (0.01) and a negative Δf_k value (-0.008). The favorite nucleophilic site for molecule A4 is atom C5 (Table S3) with the highest value of f_k^+ (0.104) and a positive Δf_k value (0.095), while the favorite electrophilic site is atom C7 with f_k^- (0.07) and a negative Δf_k value (-0.006). The favorite nucleophilic site for molecule A5 is atom C8 (Table S4) with the highest value of f_k^+ (0.447) and a positive Δf_k value (0.46) while the favorite electrophilic site is atom C7 with f_k^- (0.443) and a negative Δf_k value (-1). The favorite nucleophilic site for molecule A6 is atom C5 (Table S5) with the highest value of f_k^+ (0.105) and a positive Δf_k value (0.99) while the favorite electrophilic site is atom C13 with f_k^- (0.009) and a negative Δf_k value (-0.006).

For B1-B6, the favorite nucleophilic sites for molecule B1 are atoms N1 and N4 (Table S6) with the highest values of f_k^+ (0.022 each) and positive Δf_k values (0.024 and 0.025, respectively), while the favorite electrophilic site is atom C5 with f_k^- (0.074) and a negative Δf_k value (-0.069). The favorite nucleophilic site for molecule B2 is atom N1 (Table S7) with the highest values of f_k^+ (0.015) and a positive Δf_k value (0.026), while the favorite electrophilic sites are atoms C5 and C21 with f_k^- value of (0.025 each) and negative Δf_k values (-0.022 and -0.025, respectively). The favorite nucleophilic site for molecule B3 is atom N1 (Table S8) with the highest value of f_k^+ (0.02) and a positive Δf_k value (0.02) while the favorite electrophilic site is atom C10 with f_k^- value of (0.539) and a negative Δf_k value (-0.575). The favorite nucleophilic site for molecule B4 is atom N1 (Table S9) with the highest value of f_k^+ (0.018) and a positive Δf_k value (0.02), while the favorite electrophilic site is atom C15 with f_k^- value of (0.369) and a negative Δf_k value (-0.771). The favorite nucleophilic site for molecule B5 is atom C9 (Table S10) with the highest value of f_k^+ (0.067) and a positive Δf_k value (0.111), while the favorite electrophilic site is atom C5 with f_k^- value of (0.067) and a negative Δf_k value (-0.062). The favorite nucleophilic site for molecule B6 is atom N1 (Table S11) with the highest value of f_k^+ (0.017) and a positive Δf_k value (0.02), while the favorite electrophilic site is atom C5 with f_k^- value of (0.483) and a negative Δf_k value (-1.036). In essence, the nucleophilic and electrophilic sites on the corrosion inhibitors are located on different carbon atoms for effective metal-inhibitor interactions.

Monte Carlo simulation

The total energy of iron-inhibitor (E_{Tot}) and adsorption energy (E_{Ads}), which is a sum of the rigid adsorption energy (E_{Rigid}) and the deformation energy (E_{Def}) were calculated (Table 3). E_{Tot}, a measure of stability of the substrate-adsorbate systems is in the order: Fe(110)-A6 <

Table 3 Monte Carlo simulation results for Fe(110)-inhibitor systems for all compounds (All energies are in kcal/mol). E_{Tot} = Total energy, E_{Ads} = Adsorption energy, E_{Rig} = Rigid adsorption energy, E_{Def} = Deformation energy.

System	E_{Tot}	E_{Ads}	E_{Rig}	E_{Def}
Fe(110)-A1	-11266.02	-13257.7	-11553.4	-1704.3
Fe(110)-A2	-11276.45	-13281.3	-11584.8	-1696.5
Fe(110)-A3	-11290.40	-13290.1	-11604.3	-1685.7
Fe(110)-A4	-11188.26	-13174.6	-11460.3	-1714.2
Fe(110)-A5	-11106.14	-13095.0	-11393.7	-1701.2
Fe(110)-A6	-11337.98	-13313.2	-11600.0	-1713.2
Fe(110)-B1	-11323.03	-13231.6	-11519.3	-1712.2
Fe(110)-B2	-11101.56	-13026.4	-11299.1	-1727.3
Fe(110)-B3	-11143.26	-13045.3	-11332.9	-1712.3
Fe(110)-B4	-11247.01	-13166.5	-11451.4	-1712.2
Fe(110)-B5	-11331.17	-13235.1	-11527.6	-1707.4
Fe(110)-B6	-11243.56	-13142.7	-11422.8	-1719.8

Fe(110)-B5 < Fe(110)-B1 < Fe(110)-A3 < Fe(110)-A2 < Fe(110)-A1 < Fe(110)-B4 < Fe(110)-B6 < Fe(110)-A4 < Fe(110)-B3 < Fe(110)-A5 < Fe(110)-B2. The values displayed for E_{tot} show that the adsorption of molecules to the metal surface is thermodynamically favored. Low adsorption E_{Ads}, as observed in all compounds is associated with a strong adsorption of the inhibitor molecules on Fe(110) surface [36, 37]. Fig. 3 and S12-22 show the top and side views of the adsorbed molecules on the surface of Fe(110) in an aqueous solution, with all molecules arranged parallel on the plane of Fe(110) and providing good coverage on the surface. This shows that the molecules can bind to the metal surface via covalent and non-bonded interactions [38], buttressed by the negative values of $\Delta E_{back\text{-}donation}$ [28].

Conclusions

The corrosion inhibition potentials of some derivatives of triazolopyrimidinone were investigated via the density functional theory approach and Monte Carlo simulations. The electronic properties and global and local reactivity descriptors were calculated to ascertain the reactivity, stability and reactive sites of the molecules. Adsorption locator calculation was done to obtain the total energy and adsorption energy of the molecules on Fe(110) surface. The results revealed the existence of donor and acceptor parts in the molecules. Low energy band gap values were observed for the nitro substituted derivatives, as observed in the results of previous researchers. Negative $\Delta E_{back-donation}$ values in the molecules suggest charge transfer between them and the metal surface via back-donation. The E_{tot} values suggest thermodynamically favored adsorption between the molecules and the metal surface. These molecules could be used as anti-corrosive agents.

Conflict of interest

The authors declare no conflict of interest.

References

[1] Verma C, Ebenso EE, Quraishi MA, Hussain CM. Recent developments in sustainable corrosion inhibitors: design, performance and industrial scale applications. Mater Adv 2021; 2:3806–3850.

[2] Fayomi OSI, Akande IG, Odigie S. Economic Impact of Corrosion in Oil Sectors and Prevention: An Overview. J Phys 2019; 1378:1–8

[3] Raghavendra N, Bhat IB. Corrosion inhibition property of Mangala dry arecanut seed extract on mild steel surface in hydrochloric acid environment. Sci Lett 2019; 7(2):84-90.

[4] Othman MH, Al-Amiery AA, Al-Majedy YK, Amir, A, Kadhum H, Bakar A, et al. Synthesis and characterization of a novel organic corrosion inhibitor for mild steel in 1M hydrochloric acid. Res Phys 2018; 8:728–733.

[5] Peme T, Olasunkanmi LO, Bahadur I, Adekunle AS, Kabanda MM, Ebenso EE. Adsorption and corrosion inhibition studies of some selected dyes as corrosion inhibitors for mild steel in acidic medium: gravimetric, electrochemical, quantum chemical studies and synergistic effect with iodide ions. Molecules 2015; 20:16004–16029.

[6] Panteleeva M. Effective modern methods of protecting metal road structures from corrosion. IOP Conf Ser: Earth Environ Sci 2017; 90:1–6.

[7] Odewole OA, Ibeji CU, Oluwasola HO, Oyeneyin OE, Akpomie KG, Ugwu CM, et al. Synthesis and anti-corrosive potential of Schiff bases derived 4-

nitrocinnamaldehyde for mild steel in HCl medium: Experimental and DFT studies. J Mol Struct 2021; 1223:129214.
[8] Akinyele OF, Adekunle AS, Olayanju DS, Oyeneyin OE, Durodola SS, et al. Synthesis and corrosion inhibition studies of (E)-3-(2-(4-chloro-2-nitrophenyl)diazenyl)-1-nitrosonaphthalen-2-ol on mild steel dissolution in 0.5 M HCl solution-experimental, DFT and Monte Carlo simulations. J Mol Struct 2022; 1268:133738.
[9] Finsgar M, Jackson J. Application of corrosion inhibitors for steels in acidic media for the oil and gas industry : A review. Corr Sci 2014; 86:7–41.
[10] Chen L, Lu D, Zhang Y. Organic compounds as corrosion inhibitors for carbon steel in HCl solution: a comprehensive review. Matter 2022; 15: 1–59.
[11] Ramaganthan B, Gopiraman M, Olasunkanmi LO, Kabanda MM, Yesudass S, Bahadur I, et al. Synthesized photo-cross-linking chalcones as novel corrosion inhibitors for mild steel in acidic medium: experimental, quantum chemical and Monte Carlo simulation studies. RSC Adv 2015; 5:1–47.
[12] Oyeneyin O, Akerele D, Ojo N, Oderinlo O. Corrosion inhibitive Potentials of some 2H-1-benzopyran-2-one derivatives-DFT calculations. Biointer Res Appl Chem 2021; 11:13968–13981.
[13] Chuan L, Bin X, Like Z, Xingwen Z, Xiao M, Shasha Z. Adsorption and corrosion inhibition of mild steel in hydrochloric acid solution by S-allyl- O,O'-dialkyldithiophosphates. Res Phys 2017; 7:3434–3443.
[14] Cherif M, Horchani M, Al-Ghamdi YO, Almalki SG, Alqurashi YE, Jannet HB, Romdhane A. New prano-1,2,3-triazolopyrimidinone derivatives as anticholinesterase and antibacterial agents: Design, microwave-assisted synthesis and molecular docking study. J Molec Struct 2020; 1220:128685.
[15] Zacarías NVO, van Veldhoven JPD, den Hollander LS, Dogan B, Openy J, Hsiao Y, et al. Synthesis and pharmacological evaluation of triazolopyrimidinone derivatives as noncompetitive, intracellular antagonists for CC chemokine receptors 2 and 5. J Medic Chem 2019; 62:11035–11053.
[16] Istanbullu H, Bayraktar G, Ozturk I, Coban G, Saylam M. Design, synthesis and bioactivity studies of novel triazolopyrimidinone compounds. J Res Pharm 2022; 26:231–242.
[17] Obot IB, Macdonald DD, Gasem ZM. Density Functional Theory (DFT) as a powerful tool for designing new organic corrosion inhibitors. Part 1: An overview. Corr Sci 2015; 99:1-30.
[18] Omoboyowa DA, Singh G, Fatoki JO, Oyeneyin OE. Computational investigation of phytochemicals from Abrus precatorius seeds as modulators of peroxisome proliferator-activated receptor gamma (PPARγ). J Biomolec Struct Dynam 2022; 40:1–15.
[19] Ojo ND, Krause RW, Obi-Egbedi NO. Electronic and nonlinear optical properties of 3-(((2-substituted-4-nitrophenyl)imino)methyl)phenol. Computat Theor Chem 2020; 1192:1–8.
[20] Amoko SJ, Akinyele OF, Oyeneyin OE, Olayanju DS, Aboluwoye CO. Experimental and theoretical investigation of corrosion inhibitive potentials of (E)-4-hydroxy-3-[(2,4,6-tribromophenyl)diazenyl] benzaldehyde on mild steel in acidic media. Phys Chem Res 2020; 8:399–416.
[21] El Attari H, Mengouch S, Siniti M, Zahidi E, Khamliche L, Kheribech A. Quantum chemical studies and adsorption characteristic of 4-hydroxy-3-[1-(2-phenylhydrazinylidene)ethyl]2h-1 benzopyran-2-one on mild steel in hydrochloric acid. J Mater Environ Sci 2018; 9:689–700.
[22] Kumar D, Ech-chihbi E, El-hajjaji F. Investigations on some coumarin based corrosion inhibitors for mild steel in aqueous acidic medium: electrochemical, surface morphological, density functional theory and Monte Carlo simulation approach. J Mol Liq 2021; 329:115531.
[23] Shao Y, Molnar LF, Jung Y, Kussmann J, Ochsenfeld C, Brown ST, et al. SPARTAN 14, build 1.01. Irvine (CA); 2014.
[24] Becke AD. Density-functional thermochemistry. III. The role of exact exchange. J Chem Phys 1993; 98:5648-5652.
[25] Oyeneyin OE, Adejoro IA, Obadawo BS, Amoko JS, Kayode IO, Akintemi EO, et al. Investigation into the molecular properties of 3-(4-hydroxyphenyl) prop-2-en-1-one 4-phenyl Schiff base and some of its derivatives-DFT and molecular docking studies. Sci Lett 2021; 9(1):4-11.
[26] Parr RG, Hill C, Carolina N. Electrophilicity Index. J Amer Chem Soc 1999; 121:1922–1924.
[27] Rahimi A, Abdouss M, Farhadian A, Guo L, Neshati J. Development of a novel thermally stable inhibitor based on furfuryl alcohol for mild steel corrosion in a 15% HCl medium for acidizing application. Indust Engineer Chem Res 2021; 60:11030–11044.
[28] Haldhar R, Prasad D, Bahadur I, Dagdag O, Kaya S, Verma DK, Kim S. Investigation of plant waste as a renewable biomass source to develop efficient, economical and eco-friendly corrosion inhibitor. J Mol Liq 2021; 335:116184.
[29] Obot IB, Kaya S, Kaya C, Tuzun B. Theoretical evaluation of triazine derivatives as steel corrosion inhibitors: DFT and Monte Carlo simulation approaches. Res Chem Inter 2016; 42:4963-4983.
[30] Saravanan C, Nasrin IS, Millind SD. Electron withdrawing substituent that control band gap and planar conformation in push-pull molecules through non-covalent interactions: density functional theory study. Res Rev J Chem 2018; 7:20–30.
[31] Ojo ND, Krause RW, Obi-Egbedi NO. Electronic and nonlinear optical properties of 2-(((5-aminonaphthalen-1-yl)imino)methyl)phenol: experimental and time-dependent density functional studies. J Molec Liq 2020; 319:11415.
[32] Geerlings P, De Proft F. Chemical reactivity as described by quantum chemical methods. Inter J Molec Sci 2002; 3:276–309.
[33] Albrakaty RH, Wazzan NA, Obot IB. Theoretical study of the mechanism of corrosion inhibition of carbon steel in acidic solution by 2-aminobenzothaizole and 2-mercatobenzothiazole. Inter J Electro Sci 2018; 13:3535–3554.

[34] Targema M, Obi-Egbedi NO, Adeoye MD. Molecular structure and solvent effects on the dipole moments and polarizabilities of some aniline derivatives. Computat Theor Chem 2013; 1012:47–53.
[35] Ogunyemi BT, Latona TF, Ayinde AA, Adejoro IA. Theoretical investigation to corrosion inhibition efficiency of some chloroquine derivatives using density functional theory. Adv J Chem-Sect A 2020; 3:485-492.
[36] Rahimi A, Abdouss M, Farhadian A, Guo L, Neshati J. Development of a novel thermally stable inhibitor based on furfuryl alcohol for mild steel corrosion in a 15% HCl medium for acidizing application. Indus Engineer Chem Res 2021; 60:11030–11044.
[37] Ojo FK, Adejoro IA, Lori JA, Oyeneyin OE, Akpomie KG. Indole derivatives as organic corrosion inhibitors of low carbon steel in HCl medium-experimental and theoretical approach. Chem Afr 2022; doi: 10.1007/s42250-022-00378-5.
[38] Loto R. Surface coverage and corrosion inhibition effect of Rosmarinus officinalis and zinc oxide on the electrochemical performance of low carbon steel in dilute acid solutions. Res Phys 2018; 8:172– 179.